A sub-domain smoothed Galerkin method for solid mechanics problems

Dean Hu[1, 2], Yigang Wang[1], G. R. Liu[3], Tong Li[2], Xu Han[1] and Y. T. Gu[2,*]

[1]*State Key Laboratory of Advanced Design and Manufacturing for Vehicle Body, Hunan University, Changsha 410082, P. R. China*

[2]*School of Chemistry, Physics and Mechanical Engineering, Queensland University of Technology, GPO Box 2434, Brisbane, QLD 4001, Australia*

[3]*School of Aerospace Systems, University of Cincinnati, 2851 Woodside Dr, Cincinnati, OH 45221, USA*

[*]*E-mail address: yuantong.gu@qut.edu.au (Y.T. Gu)*

Abstract: A sub-domain smoothed Galerkin method is proposed to integrate the advantages of mesh-free Galerkin method and Finite Element Method (FEM). Arbitrarily shaped sub-domains are predefined in problems domain with mesh-free nodes. In each sub-domain, based on mesh-free Galerkin weak formulation, the local discrete equation can be obtained by using the Moving Kriging (MK) interpolation, which is similar to the discretization of the high-order finite elements. Strain smoothing technique is subsequently applied to the nodal integration of sub-domain by dividing the sub-domain into several smoothing cells. Moreover, condensation of degree of freedom can also be introduced into the local discrete equations to improve the computational efficiency. The global governing equations of present method are obtained based on the scheme of FEM by assembling all local discrete equations of the sub-domains. The mesh-free properties of Galerkin method are retained in each sub-domain. Several 2D elastic problems have been solved based on this newly proposed method to validate its computational performance. These numerical examples proved that the newly proposed sub-domain smoothed Galerkin method is a robust technique to solve solid mechanics problems based on its characteristics of high computational efficiency, good accuracy and convergence.

Keywords: Galerkin method; mesh-free method; FEM; MK interpolation; strain smoothing technique; condensation of degree of freedom

1. Introduction

For several decades, Finite Element Method (FEM) has become one of the most popular numerical tools in solving practical problems in aeronautical, mechanical and civil engineering. However, the shape of element in FEM cannot be distorted too much due to the use of weak formulations that require mapping for the integration [1, 2]. In order to avoid numerical problems related to element distortion encountered in FEM, the development and application of mesh-free methods has attracted much attention in the recent two decades. The key advantage of mesh-free method is that only nodal information is required and no element connectivity is needed, which leads to the versatility of mesh-free method for engineering problems with complex geometry [3, 4].

The Element-Free Galerkin (EFG) method, which is originated by Belytschko et al. [5-8] based on Moving Least-Squares (MLS) interpolation, is one of the most widely used earlier mesh-free methods. The shape functions constructed by MLS interpolation, which do not have the property of Kronecker delta function, make it hard to treat the essential boundary conditions. Therefore, many special techniques have been proposed to impose essential boundary conditions, such as Lagrange multipliers, singular weighting functions and penalty method [4, 9-11]. However, these methods still need additional efforts to enforce the essential boundary conditions. In order to fully eliminate the difficulties associated with EFG method for imposing essential boundary conditions, Liu and

Gu have developed the Point Interpolation Methods (PIM) by using polynomial basis or/and Radial Basis Function (RBF) [12-15]. Lei Gu has introduced the Moving Kriging (MK) interpolation-based mesh-free method for solving simple steady-state heat conduction problems [16]. In the PIM and MK interpolation, the shape functions with the Kronecker delta function property can be obtained, and the essential boundary conditions can be imposed directly as the FEM. A comparison between the Radial Point Interpolation Method (RPIM) and the Kriging interpolation is developed by Dai et al. for elastic problems [17]. They concluded that the RPIM interpolation is similar to the Kriging interpolation theoretically. Moreover, Lam et al. has introduced a Local Kriging (LoKriging) method for two-dimensional solid mechanics problems [18], and Li et al. has further developed the LoKriging method to be used in structural dynamics analysis [19]. Moreover, a moving Kriging interpolation-based element-free Galerkin method is developed by Bui et al. for static analysis, structural dynamic analysis and free vibration analysis of Kirchhoff plates [20-22].

On the other hand, Gauss integration is commonly used in mesh-free Galerkin methods based on weak formulation, which increase the computational cost in simulation due to its complexity. Dolbow and Belytschko illustrated the error of Gauss integration by using the element-free Galerkin method, and developed integration cells which can reduce quadrature error [23]. Beissel and Belytschko proposed a direct nodal integration method that can eliminate the background mesh for integration in the element-free Galerkin framework [24]. However, direct nodal integration is usually numerical instability and of low computational accuracy. Bonet and Krongauz et al. found that the reason of low computational accuracy is caused by the violation of the integration constrain (IC) in the Galerkin weak formulations and an integral correction is introduced to improve the accuracy of nodal integration [25, 26]. Furthermore, Chen et al. introduced a strain smoothing technique into nodal integration for stabilization, which computes nodal strain by a divergence counterpart of spatial averaging of strain [27-29]. The nodal integration using strain smoothing technique for mesh-free Galerkin method shows high accuracy and convergent properties.

For mesh-free methods based on nodal integration, the entire domain is still required to be discretized into cells based on the field nodes for the purpose of integration, such as Voronioi diagram. Liu et al. proposed a Smoothed Finite Element Method (S-FEM) by introducing the strain smoothing technique into the standard FEM framework, in which the cells for integration are divided based on elements [30-32]. The S-FEM of general *n*-sided polygonal elements has been formulated, and works particularly well for very heavily distorted mesh of arbitrary shaped elements [33]. Liu et al. also gave detailed theoretical aspects including stability, bound property and convergence about S-FEM [31]. Liu et al. extended the S-FEM for large deformation analysis [34]. Nguyen-Xuan et al. extend the S-FEM for plate problem by coupling with MITC4 element [35]. All these models have a common foundation of the so-called G space theory and fall into the category of weakened weak (W^2) formulation [36, 37]. The S-FEM is more efficient than mesh-free Galerkin methods that are based on nodal integration, because the predefined elements with node connectivity are used for interpolation, integration and assembling the global system equations in S-FEM. The local discrete equations based on element are one of the reasons to improve the computational efficiency in mesh-based method [38].

However, as discussed above, the S-FEM is developed based on the standard FEM framework, the elements with node connectivity is not convenient and flexibility for the adaptive mesh refinement compared with mesh-free method, because no element connectivity is required besides nodal information in discrete process of the mesh-free method. We note that the sub-domains divided from problem domain by domain decomposition

methods are usually used for isogeometric analysis [39] and parallel computing [40, 41]. The refinement methods can be applied to single sub-domain independently with no regard to other sub-domains in isogeometric analysis. For parallel computing, a complex large problem is also preferred to be solved in smaller sub-domains independently by exchanging overlap region data or information among conjoint sub-domains. In this paper, the sub-domains divided from the entire problem domain are used to integrate the advantages of mesh-free Galerkin method and FEM. The sub-domains are predefined in the problem domain with arbitrary shape as similar as the discrete process of FEM, but mesh-free nodes are distributed in sub-domains and the domain boundaries. Local discrete equation obtained by MK interpolation possess the properties of mesh-free method, but the scheme for assembling global system equations is similar to the FEM with high-order element. Finally, the nodal integration with strain smoothing technique and condensation technique can also be implemented into present method based on the sub-domains. Condensation technique is used to reduce the degree of freedom by transferring displacements of inner nodes to displacements of boundary nodes in system equations, which is usually used in FEM to improve the computational efficiency of problems with enormous number of degree of freedom [42, 43].

The outline of this paper is as follows. The sub-domains with mesh-free nodes are described in Section 2. In Section 3, a brief summary of MK interpolation is given. The strain smoothing technique based on sub-domain is presented in Section 4. In Section 5, we present the elastic static formulations of sub-domain smoothed Galerkin method by integrating the strain smoothing technique and the condensation technique of degree of freedom. The Compatibility and Convergence of present method is also discussed in Section 5. In Section 6, some numerical examples are investigated and discussed to validate the performance of the present method. Finally, some conclusions are given in Section 7.

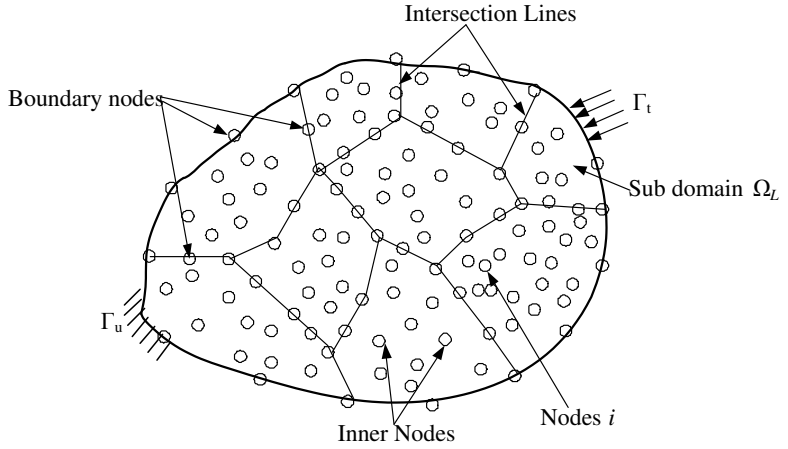

Figure 1. Sub-domains with nodes in problem domain

2. Sub-domains with mesh-free nodes

Considering a 2D problem with the domain of Ω and the boundary of Γ, as shown in Figure 1, the problem domain can be divided into sub-domains as similar as the discrete process in FEM. Then scattered nodes are distributed in sub-domains and their boundaries. If a sub-domain Ω_L intersects with its adjacent sub-domain Ω_K, they connect each other with the intersection line Γ_{IL} without overlapping. The intersection line can be of arbitrary morphology, such as straight, curve, polygonal line. The union of all sub-domains can cover the entire problem domain of Ω, which yields

$$\Omega = \bigcup_{L=1}^{M} \Omega_L \ , \quad L = 1, 2 \cdots M \tag{1}$$

and Γ_L is the boundary of sub-domain Ω_L, it is combined by

$$\Gamma_L = \Gamma_{\mathrm{I}L} \cup \Gamma_{\mathrm{t}L} \cup \Gamma_{\mathrm{u}L} \tag{2}$$

where M is the total number of sub-domains in the problem domain. $\Gamma_{\mathrm{t}L}$ and $\Gamma_{\mathrm{u}L}$ respectively denotes the part of natural boundary and essential boundary that intersects with sub-domain Ω_L. $\Gamma_{\mathrm{I}L}$ is the intersection line between neighboring sub-domains. Scattered nodes at boundary Γ_L are referred to as boundary nodes, and nodes in sub-domain Ω_L are referred to as inner nodes, as shown in Figure 1.

In this paper, sub-domain smoothed Galerkin method is formulated based on mesh-free Galerkin method and implemented with the scheme of FEM. The essence of present method is as follows. (1) The local discrete formulation based on mesh-free Galerkin weak form is established over each sub-domain by using MK interpolation, in which nodes within the sub-domain are used for approximation. Then, local search of neighboring nodes for interpolation is implemented in each sub-domain. (2) Integration is performed on the basis of sub-domains. Each sub-domain may be further subdivided into several smoothing cells (SC). Then, a strain smoothing operation is performed for integration of each smoothing cell within the sub-domain. (3) Local discrete formulation based on sub-domains can be simplified by the condensation of degree of freedom, which transfers equations of inner nodes to equations of boundary nodes. The formulations of sub-domain smoothed Galerkin method are detailed in following sections.

3. Moving kriging interpolation

Considering a sub-domain Ω_L, which is the neighborhood of point $\mathbf{x}$, is located in the problem domain Ω. MK interpolation for approximation of field variable u can be defined as [16]

$$u^h(\mathbf{x}) = [\mathbf{p}^{\mathrm{T}}(\mathbf{x})\mathbf{A} + \mathbf{r}^{\mathrm{T}}(\mathbf{x})\mathbf{B}]\mathbf{u} = \sum_{I=1}^{n} \Phi_I(\mathbf{x}) u_I \tag{3}$$

where n is the total number of nodes for interpolation. $\Phi_I(\mathbf{x})$ is the MK shape functions and is defined as

$$\Phi_I(\mathbf{x}) = \sum_{j=1}^{m} p_j(\mathbf{x}) A_{jI} + \sum_{k=1}^{n} r_k(\mathbf{x}) B_{kI} \tag{4}$$

in which A_{jI} is the (j, I) element of matrix $\mathbf{A}$, and B_{kI} is the (k, I) element of matrix $\mathbf{B}$. Matrixes $\mathbf{A}$ and $\mathbf{B}$ can be written as the following

$$\mathbf{A} = (\mathbf{P}^{\mathrm{T}}\mathbf{R}^{-1}\mathbf{P})^{-1}\mathbf{P}^{\mathrm{T}}\mathbf{R}^{-1} \tag{5a}$$

$$\mathbf{B} = \mathbf{R}^{-1}(\mathbf{I} - \mathbf{P}\mathbf{A}) \tag{5b}$$

where $\mathbf{I}$ is a unit matrix. $\mathbf{P}$ is an $n \times m$ matrix and represents the collected values of vector $\mathbf{p}(\mathbf{x})$ at the neighboring interpolated nodes of $\mathbf{x}$. Vector $\mathbf{p}(\mathbf{x})$ is the polynomial with m basis functions

$$\mathbf{p}(\mathbf{x}) = \left\{ p_1(\mathbf{x}) \ \ p_2(\mathbf{x}) \ \ \cdots \ \ p_m(\mathbf{x}) \right\}^{\mathrm{T}} \tag{6}$$

The quadratic basis functions $\mathbf{p}(\mathbf{x})=[1\ x\ y\ x^2\ y^2\ xy]^{\mathrm{T}}$ are used for numerical computations in this work. And vector $\mathbf{r}(\mathbf{x})$ in Equation (3) is

$$\mathbf{r}(\mathbf{x})=\left\{R(\mathbf{x}_1,\mathbf{x})\ \ R(\mathbf{x}_2,\mathbf{x})\ \ \cdots\ \ R(\mathbf{x}_n,\mathbf{x})\right\}^{\mathrm{T}} \tag{7}$$

where $R(\mathbf{x}_i,\mathbf{x})$ is the correlation function between the neighboring nodes $\mathbf{x}_i$ and $\mathbf{x}$, it belongs to the covariance of field value $\mathbf{u}(\mathbf{x})$. The correlation matrix $\mathbf{R}$ with size $n\times n$ is given by

$$\mathbf{R}[R(\mathbf{x}_i,\mathbf{x}_j)]=\begin{bmatrix} 1 & R(\mathbf{x}_1,\mathbf{x}_2) & \ldots & R(\mathbf{x}_1,\mathbf{x}_n) \\ R(\mathbf{x}_2,\mathbf{x}_1) & 1 & \ldots & R(\mathbf{x}_2,\mathbf{x}_n) \\ \ldots & \ldots & \ldots & \ldots \\ R(\mathbf{x}_n,\mathbf{x}_1) & R(\mathbf{x}_n,\mathbf{x}_2) & \ldots & 1 \end{bmatrix} \tag{8}$$

Many different correlation functions can be used for $\mathbf{R}$. In this paper, a Gaussian function is used

$$R(\mathbf{x}_i,\mathbf{x}_j)=e^{-\lambda r_{ij}^2} \tag{9}$$

in which $r_{ij}=\left\|\mathbf{x}_i-\mathbf{x}_j\right\|$, λ >0 is a correlation parameter. As studied in the previous work [16-19], the correlation parameter has a significant effect on the solution. In this work, $\lambda=10.0$ is employed.

The partial derivatives of $\Phi_I(\mathbf{x})$ against x_i can be obtained as following

$$\Phi_{I,i}(\mathbf{x})=\sum_{j=1}^{m}p_{j,i}(\mathbf{x})A_{jI}+\sum_{k=1}^{n}r_{k,i}(\mathbf{x})B_{kI} \tag{10}$$

where the index following a comma is a spatial derivative.

The accuracy of mesh-free methods depends on the number of nodes for interpolation. In the previous works by authors [5-8], the number of nodes for interpolation is determined in the entire problem domain by global searching of influence domain with a specified radius. The number of interpolated nodes may vary with the change of interest point **x**. In this paper, the number of nodes for interpolation is not a variable. It is only determined by the n nearest neighboring nodes of **x** in the same sub-domain Ω_L with local searching. Thus, considerable CPU time can be reduced since the neighbor searching is localized in each sub-domain instead of the entire problem domain. On the other hand, in order to ensure the nodes for interpolation are sufficient in every sub-domain, the total number of nodes in each sub-domain and its boundary should be no less than the number of nodes for interpolation. It means that the number of sub-domains is restricted by the number of interpolation nodes, when the total number of nodes is not changed in the entire problem domain.

4. Strain smoothing technique

For 2D problems, as shown in Figure 2, a sub-domain Ω_L with boundary Γ_L is divided into a number of smoothing cells. The smoothing cells are constructed by linking the center of sub-domain Ω_L with the midpoint of the lines of boundary Γ_L. If more smoothing cells are needed to be divided from the sub-domain Ω_L, smoothing cells can be further constructed by linking the center of smoothing cell Ω_L^k with the midpoint of the

segments of boundary Γ_L^k, in which Γ_L^k is the boundary of smoothing cell Ω_L^k.

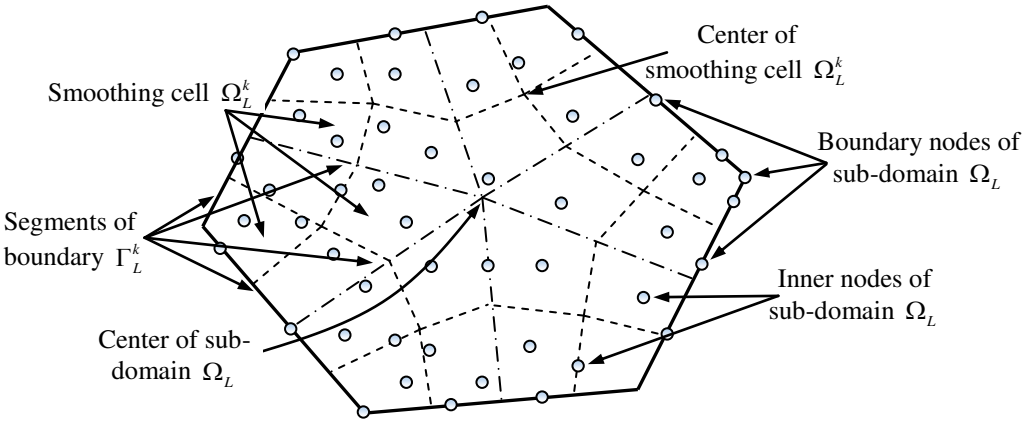

Figure 2. Smoothing cells of sub-domain Ω_L

A strain smoothing operation proposed by Chen et al. [27] is performed for sub-domain Ω_L by

$$\tilde{\varepsilon}_{ij}^h\left(\mathbf{x}_L^k\right)=\int_{\Omega_L}\tilde{\varepsilon}_{ij}^h\left(\mathbf{x}\right)\Psi\left(\mathbf{x};\mathbf{x}-\mathbf{x}_L^k\right)\mathrm{d}\Omega \tag{11}$$

where $\tilde{\varepsilon}_{ij}^h$ is the strain obtained from displacement by

$$\tilde{\varepsilon}_{ij}^h=\left(u_{i,j}^h+u_{j,i}^h\right)/2 \tag{12}$$

and Ψ is a smoothing function. For simplicity, a piecewise constant function is applied

$$\Psi\left(\mathbf{x};\mathbf{x}-\mathbf{x}_L^k\right)=\begin{cases}1/A_L^k & \mathbf{x}\in\Omega_L^k\\ 0 & \mathbf{x}\notin\Omega_L^k\end{cases} \tag{13}$$

where $A_L^k=\int_{\Omega_L^k}\mathrm{d}\Omega$ is the area of smoothing cell Ω_L^k within the sub-domain Ω_L.

Substituting Equations (12) and (13) into Equation (11) and applying the divergence theorem, the following equation is obtained

$$\begin{aligned}\tilde{\varepsilon}_{ij}^h\left(\mathbf{x}_L^k\right)&=\int_{\Omega_L}\frac{1}{2}\left(\frac{\partial u_i^h}{\partial x_j}+\frac{\partial u_j^h}{\partial x_i}\right)\Psi\left(\mathbf{x};\mathbf{x}-\mathbf{x}_L^k\right)\mathrm{d}\Omega\\&=\frac{1}{2A_L^k}\int_{\Omega_L^k}\left(\frac{\partial u_i^h}{\partial x_j}+\frac{\partial u_j^h}{\partial x_i}\right)\mathrm{d}\Omega\\&=\frac{1}{2A_L^k}\int_{\Gamma_L^k}\left(u_i^h n_j+u_j^h n_i\right)\mathrm{d}\Gamma\end{aligned} \tag{14}$$

It should be noted that the choice of constant function of Ψ makes vanishing of area integration in smoothing cell Ω_L^k, and only line integration along the boundary Γ_L^k of smoothing cell Ω_L^k is needed in Equation (14).

Substituting Equation (3) into Equation (14) , which yields

$$\tilde{\boldsymbol{\varepsilon}}^h\left(\mathbf{x}_L^k\right)=\sum_{I=1}^{n}\tilde{\mathbf{B}}_I\left(\mathbf{x}_L^k\right)\mathbf{u}_I=\tilde{\mathbf{B}}\mathbf{u} \tag{15}$$

where $\tilde{\mathbf{B}}_I$ is smoothing strain matrix. For 2D problems

$$\tilde{\boldsymbol{\varepsilon}}^{h\mathrm{T}}=\left[\tilde{\varepsilon}_{11}^h \quad \tilde{\varepsilon}_{22}^h \quad 2\tilde{\varepsilon}_{12}^h\right] \tag{16}$$

$$\mathbf{u}_I^{\mathrm{T}}=\left[u_{1I} \quad u_{2I}\right] \tag{17}$$

$$\tilde{\mathbf{B}}_I\left(\mathbf{x}_L^k\right)=\begin{bmatrix}\tilde{b}_{I1}(\mathbf{x}_L^k) & 0\\ 0 & \tilde{b}_{I2}(\mathbf{x}_L^k)\\ \tilde{b}_{I2}(\mathbf{x}_L^k) & \tilde{b}_{I1}(\mathbf{x}_L^k)\end{bmatrix} \tag{18}$$

$$\tilde{b}_{Ii}\left(\mathbf{x}_L^k\right)=\frac{1}{A_L^k}\int_{\Gamma_L^k}\Phi_I\left(\mathbf{x}\right)n_i\left(\mathbf{x}\right)\mathrm{d}\Gamma \tag{19}$$

In order to ensure the accuracy and convergence of introducing smoothing strain technique into mesh-free Galerkin formulation with nodal integration, integration constraints need to be satisfied, which has been discussed detailed in reference [27].

For the evaluation of components $\tilde{b}_{Ii}(\mathbf{x}_L^k)$ in $\tilde{\mathbf{B}}_I(\mathbf{x}_L^k)$ by using Equation (19), a boundary integration of smoothing cell is needed. If one Gaussian point is used for line integration along each segment of boundary Γ_L^k, Equation (19) can be transformed to its algebraic form

$$\tilde{b}_{Ii}\left(\mathbf{x}_L^k\right)=\frac{1}{A_L^k}\sum_{m=1}^{N_C}\Phi_I(\mathbf{x}_L^{km})n_i(\mathbf{x}_L^{km})\,l_L^{km} \tag{20}$$

where $\mathbf{x}_L^{km}$ is the midpoint (integration point) of segment of boundary Γ_L^k, whose length and outward unit normal are denoted as l_L^{km} and $n_i(\mathbf{x}_L^{km})$, respectively. N_C is the number of segment of boundary Γ_L^k.

5. Sub-domain smoothed Galerkin method

5.1 Basic formulations

Considering a 2D problem with domain Ω and boundary Γ, its equilibrium equations can be given as

$$\sigma_{ij,j}+b_i=0 \tag{21}$$

where σ_{ij} is stress tensor, b_i is body force. The boundary conditions are given as follows

$$\sigma_i n_i=\overline{t}_i \quad \text{on } \Gamma_t \tag{22a}$$

$$u_i=\overline{u}_i \quad \text{on } \Gamma_u \tag{22b}$$

where $\overline{u}_i$ and $\overline{t}_i$ are prescribed displacement and traction on essential boundary Γ_u and natural boundary Γ_t, respectively. n_j is the outward unit normal to boundary Γ.

Equilibrium equations and boundary conditions in Equations (21) and (22) should be satisfied in every sub-domain. For the Lth sub-domain $\Omega_L (L = 1, 2, \cdots, M)$, the local variational weak formulation of equilibrium equation can be obtained as

$$\int_{\Omega_L} \delta\tilde{\varepsilon}_{ij} D_{ijkl} \tilde{\varepsilon}_{kl} \mathrm{d}\Omega - \int_{\Omega_L} \delta u_i b_i \mathrm{d}\Omega - \int_{\Gamma_{tL}} \delta u_i \overline{t}_i \mathrm{d}\Gamma = 0 \tag{23}$$

where D_{ijkl} is the matrix of material constants. Because MK interpolation ensures the Kronecker delta property of shape functions [16], the essential boundary conditions do not need to enforce by Lagrange multipliers or penalty method in Equation (23).

The local discrete equations can be obtained by substituting approximations of $\mathbf{u}^h$ and $\tilde{\boldsymbol{\varepsilon}}^h$ into weak form (23), which yields

$$\mathbf{K}^L \mathbf{u}^L = \mathbf{f}^L \tag{24}$$

where $\mathbf{K}^L$, $\mathbf{u}^L$ and $\mathbf{f}^L$ are stiffness matrix, nodal displacement and force vector of sub-domain Ω_L, separately, and are given by using nodal integration

$$\begin{aligned} \mathbf{K}_{IJ}^L &= \int_{\Omega_L} \tilde{\mathbf{B}}_I^{\mathrm{T}} \mathbf{D} \tilde{\mathbf{B}}_J \mathrm{d}\Omega \\ &= \sum_{k=1}^{N_S} \int_{\Omega_L^k} \tilde{\mathbf{B}}_I^{\mathrm{T}} \left(\mathbf{x}_L^k \right) \mathbf{D} \tilde{\mathbf{B}}_J \left(\mathbf{x}_L^k \right) \mathrm{d}\Omega \\ &= \sum_{k=1}^{N_S} \tilde{\mathbf{B}}_I^{\mathrm{T}} \left(\mathbf{x}_L^k \right) \mathbf{D} \tilde{\mathbf{B}}_J \left(\mathbf{x}_L^k \right) A_L^k \end{aligned} \tag{25a}$$

$$\mathbf{f}_I^L = \sum_{n=1}^{Nb_S} \boldsymbol{\Phi}_I^{\mathrm{T}} \left(\mathbf{x}_L^n \right) \overline{\mathbf{t}} \left(\mathbf{x}_L^n \right) s_L^n + \sum_{k=1}^{N_S} \boldsymbol{\Phi}_I^{\mathrm{T}} \left(\mathbf{x}_L^k \right) \mathbf{b} \left(\mathbf{x}_L^k \right) A_L^k \tag{25b}$$

where N_S is the total number of smoothing cells in sub-domain Ω_L. Nb_S is the total number of segment on the natural boundary Γ_{tL}, which is produced by the smoothing cells in sub-domain Ω_L. s_L^n is the weight associated with the specific segment on the natural boundary Γ_{tL}, which can be computed by the length of segments. **D** is the matrix of material constants.

Equation (24) presents linear local discrete equations for the sub-domain Ω_L. Using Equation (24) for all M sub-domains in the entire problem domain, global system equations can be obtained by assembling all local discrete equations

$$\mathbf{K}_{2n_t \times 2n_t} \mathbf{u}_{2n_t \times 1} = \mathbf{f}_{2n_t \times 1} \tag{26}$$

where n_t is the total number of nodes in the entire problem domain.

It should be noted that the assembling of global system equations based on sub-domains is the same with the scheme of FEM, the system stiffness matrix in the present method is symmetric and banded if the nodes are numbered properly by sorting sub-domains and coordinate direction. Then, as similarly discussed in FEM [1], the bandwidth of the global stiffness matrix should depend on the number of nodes in each sub-domain and the

difference of nodal number of nodes assigned to the sub-domains. The sub-domain that has the biggest difference of nodal number controls the bandwidth of the global stiffness matrix. The bandwidth can be changed even for the same model by changing the nodal number of the mesh-free nodes in sub-domains. It should be an interesting work in the future to improve the computational efficiency of present method by minimizing the bandwidth after meshing the problem domain with sub-domain and corresponding mesh-free nodes.

5.2 Condensation of degree of freedom

In order to improve the computational efficiency of present method, condensation technique of degree of freedom can be introduced to the local discrete equations (24). Discrete equations only involve expression of boundary nodes of sub-domains by transferring equations of inner nodes to equations of boundary nodes.

Suppose *P* boundary nodes and *Q* inner nodes are included in the sub-domain Ω_L, local discrete equations (24) are numbered by sorting degree of freedom of boundary nodes and inner nodes, which yields

$$\begin{bmatrix} \mathbf{K}_{PP} & \mathbf{K}_{PQ} \\ \mathbf{K}_{QP} & \mathbf{K}_{QQ} \end{bmatrix} \begin{bmatrix} \mathbf{q}_P^{\text{conn}} \\ \mathbf{q}_Q^{\text{inn}} \end{bmatrix} = \begin{bmatrix} \mathbf{f}_P^{\text{conn}} \\ \mathbf{f}_Q^{\text{inn}} \end{bmatrix} \tag{27}$$

where

$$\mathbf{q}_P^{\text{conn}} = \begin{bmatrix} u_1 & u_2 & \dots & u_P \end{bmatrix} \tag{28a}$$

$$\mathbf{q}_Q^{\text{inn}} = \begin{bmatrix} u_{P+1} & u_{P+2} & \dots & u_{P+Q} \end{bmatrix} \tag{28b}$$

Using the second formulation of Equation (27), displacements of inner nodes can be expressed as

$$\mathbf{q}_Q^{\text{inn}} = \mathbf{K}_{QQ}^{-1}[\mathbf{f}_Q^{\text{inn}} - \mathbf{K}_{QP}\mathbf{q}_P^{\text{conn}}] \tag{29}$$

Substituting Equation (29) into the first formulation of Equation (27), local discrete equations of sub-domain Ω_L are given by

$$\mathbf{K}^{\text{R}}\mathbf{q}_P^{\text{conn}} = \mathbf{f}^{\text{R}} \tag{30}$$

where

$$\mathbf{K}^{\text{R}} = \mathbf{K}_{PP} - \mathbf{K}_{PQ}\mathbf{K}_{QQ}^{-1}\mathbf{K}_{QP} \tag{31}$$

$$\mathbf{f}^{\text{R}} = \mathbf{f}_P^{\text{conn}} - \mathbf{K}_{PQ}\mathbf{K}_{QQ}^{-1}\mathbf{f}_Q^{\text{inn}} \tag{32}$$

Using Equation (30) for all *M* sub-domains in the entire problem domain, global system equations with condensation of degree of freedom can be obtained by assembling all local discrete equations

$$\mathbf{K}_{2n_b \times 2n_b}\mathbf{u}_{2n_b \times 1} = \mathbf{f}_{2n_b \times 1} \tag{33}$$

where n_b is the total number of boundary nodes of sub-domains in the entire problem domain.

5.3 Compatibility and Convergence

In the sub-domain smoothed Galerkin method, compatibility of displacements must be satisfied at the intersection line of adjacent sub-domains in 2D problems. If criterion of compatibility is satisfied, compatibility will be obtained in present method. In addition, if the criterion of completeness is also satisfied as compatibility is obtained, the computational convergence will be assured. Criterions of compatibility and completeness are described as follows, which are already proved in FEM.

Criterion of compatibility: In the equations of variational weak form, the highest order derivative of displacement function is *m*. Continuity, up to *m*−1 order derivative of displacement function, must be satisfied at the intersection line.

Criterion of completeness: In the equations of variational weak form, the highest order derivative of displacement function is *m*. Complete polynomial of *m* order must be included in the approximation functions of displacement.

For 2D elastic problems, the highest order derivative of displacement function in the weak form (23) is 1. In MK interpolation, adding complete polynomial of quadratic order can ensure reproduction of linear field. Then compatibility and completeness of present method will be satisfied. If continuity of higher derivatives are required in the problems of plate or shell, complete polynomial of higher order will ensures the compatibility and convergence of present method.

5.4 Procedure of sub-domain smoothed Galerkin method

The numerical procedure for present method is given as Table 1.

Table 1. Procedure of sub-domain smoothed Galerkin method

1. Loop over sub-domains Ω_L of problem domain Ω.
2. Loop over smoothing cells Ω_L^k in sub-domain Ω_L, compute the area A_L^k of the smoothing cell Ω_L^k.
3. Loop over midpoint (Gaussian point) $\mathbf{x}_L^{km}$ of segment of boundary Γ_L^k.
   a. Check all nodes in sub-domain Ω_L to determine the *n* nearest neighboring nodes of point $\mathbf{x}_L^{km}$.
   b. Compute $\Phi_I(\mathbf{x}_L^{km})(I=1,2,\cdots,n)$, $n_i\left(\mathbf{x}_L^{km}\right)$ and l_L^{km} at point $\mathbf{x}_L^{km}$.
4. Compute the matrix $\tilde{\mathbf{B}}_I(\mathbf{x}_L^k)$ by using Equations (20) and (18).
5. End midpoint of segment loop.
6. Evaluate local discrete equations (24) or (30) of sub-domain Ω_L for sub-domain smoothed Galerkin method without or with condensation of degree of freedom.
7. End smoothing cells loop.
8. Assemble local discrete equations of sub-domain Ω_L to obtain global system equations.
9. End sub-domains loop.
10. Implement essential boundary conditions.
11. Solve the global system equations to obtain the nodal displacements.
12. Evaluate strains and stresses at interested nodes.

6. Numerical examples

Numerical examples of 2D elastic problems are presented to analyze the performance of the proposed sub-domain smoothed Galerkin method without or with condensation of degree of freedom. All simulations are performed on a computer with an Intel(R) Core (TM) i3-2100 CPU Processor (3.10 GHz, 3.49GB) in WINDOWSXP (32-Bit Edition) operating system. The computational cost in this paper is the CPU time in all the following analysis of computational efficiency.

6.1 Cantilever beam

A cantilever beam loaded by a tangential traction on the free end, as shown in Figure 3, is now discussed. The

problem has been solved for plane stress with $E=3.0\times10^7$, $\mu=0.3$, $L=48.0$, $h=12.0$ and $F=-1000$. Numerical results of present method are compared with analytical solutions that are given by Timoshenko and Goodier [44]

$$u_x=-\frac{F}{6Eh^3}\left(y-\frac{h}{2}\right)\left[(6L-3x)x+(2+\mu)\left(y^2-2hy\right)\right] \tag{34a}$$

$$u_y=\frac{F}{6Eh^3}\left[3\mu(y^2-2hy+0.5h^2)(3L-x)x^2+0.25(4+5\mu)h^2x+(L-x/3)3x^2\right] \tag{34b}$$

For error analysis and convergence studies, error norms of displacement and energy are defined as following

$$e_u=\left[\int_\Omega 1/2\left(\mathbf{u}^{\text{Num}}-\mathbf{u}^{\text{Exact}}\right)\mathrm{D}\left(\mathbf{u}^{\text{Num}}-\mathbf{u}^{\text{Exact}}\right)\mathrm{d}\Omega\right]^{\frac{1}{2}} \tag{35}$$

$$e_e=\left[\int_\Omega 1/2\left(\boldsymbol{\varepsilon}^{\text{Num}}-\boldsymbol{\varepsilon}^{\text{Exact}}\right)\mathrm{D}\left(\boldsymbol{\varepsilon}^{\text{Num}}-\boldsymbol{\varepsilon}^{\text{Exact}}\right)\mathrm{d}\Omega\right]^{\frac{1}{2}} \tag{36}$$

where $\mathbf{u}^{\text{Num}}$ and $\boldsymbol{\varepsilon}^{\text{Num}}$ are the displacement and strain obtained by sub-domain smoothed Galerkin method, $\mathbf{u}^{\text{Exact}}$ and $\boldsymbol{\varepsilon}^{\text{Exact}}$ are those of analytical solutions.

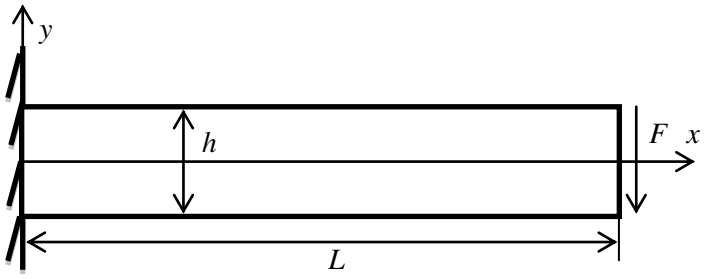

Figure 3. Cantilever beam

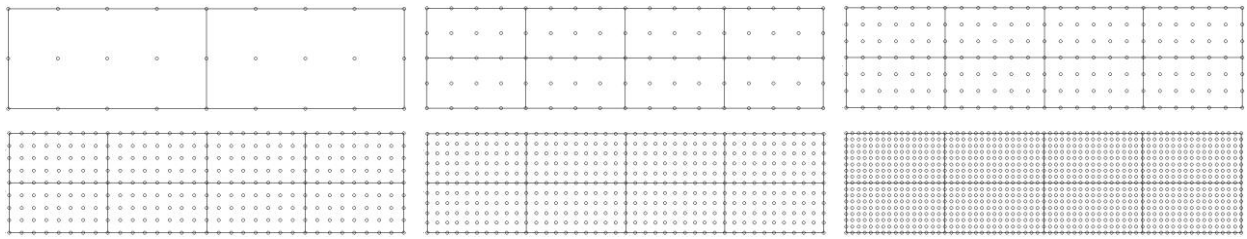

(a) Distributed nodes without condensation

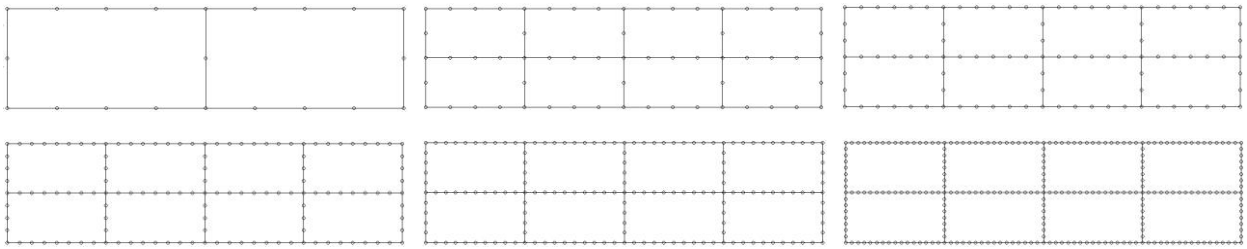

(b) Distributed nodes with condensation

Figure 4. Distributed sub-domains and nodes of cantilever beam

For analysis of computational accuracy and efficiency influenced by the present method, 27(9×3), 85(17×5), 175(25×7), 451(41×11), 637(49×13), 1105(65×17) uniformly distributed nodes and 256, 1024, 2304, 6400, 9216,

16384 quadrilateral smoothing cells are separately used in the entire problem domain, as shown in Figure 4(a), corresponding to 128, 128, 288, 800, 1152 and 2048 smoothing cells are used in each sub-domain. The number of nodes n=11 is used for MK interpolation based on sub-domains. Figure 4(b) shows the boundary nodes of sub-domains in the cantilever beam. Error norms of displacement and energy with respect to the CPU time are plotted in Figure 5. The computational performances are compared among FEM with linear triangular elements, EFG method with MK interpolation [16] and present method with condensation, where the number of degree of freedom of FEM is 170, 1274, 3402, 8514, 10730 and 22154 and the distributed nodes of EFG method with MK interpolation are 27(9×3), 85(17×5), 175(25×7), 297(33×9), 451(41×11) and 637(49×13). It can be found that the present method can use less CPU time than the linear FEM and the method in reference [16] to achieve the same level of accuracy. On the other hand, when using the same CPU time, the present method achieves a better accuracy than the linear FEM and the method in reference [16].

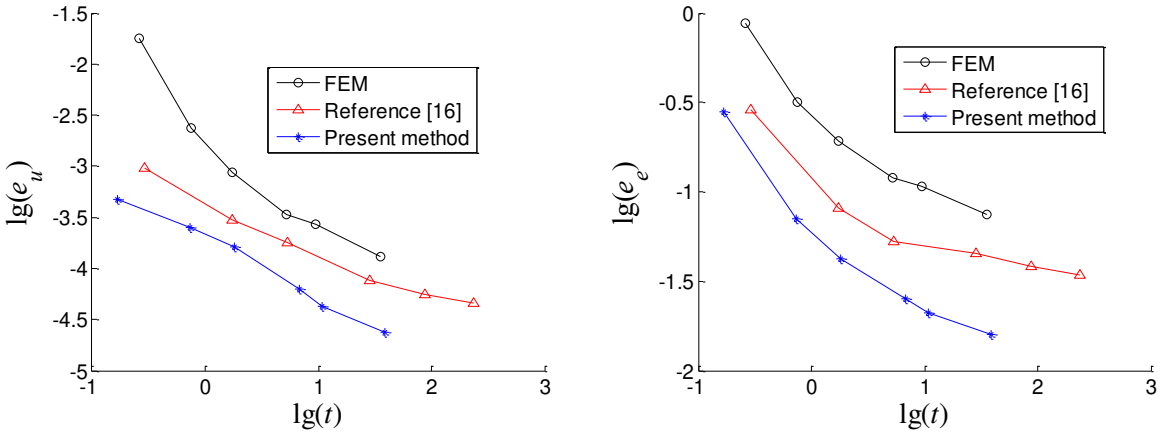

(a) Error norms of displacement (b) Error norms of energy

Figure 5. Error norms with respect to CPU time obtained by different methods

Table 2. The CPU time of present method with different number of nodes (Unit: s)

Number of nodes	27	85	175	451	637	1105
Without condensation	0.1774	0.7409	1.8491	7.3318	11.471	41.585
With condensation	0.1665	0.7281	1.7961	6.7672	10.797	38.674

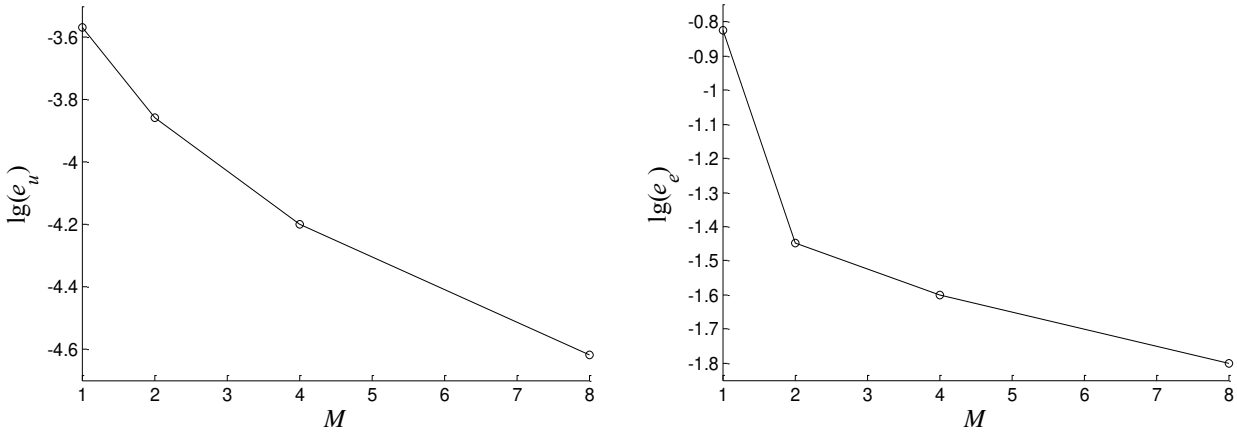

(a) Error norms of displacement (b) Error norms of energy

Figure 6. Convergence of error norms of displacement and energy

Table 2 shows the computational cost of present method with and without condensation under the different number of distributed nodes in Figure 4. It can be seen that the present method with condensation of degree of freedom can improve the computational efficiency by transferring equations of inner nodes to equations of boundary nodes.

For convergence analysis of sub-domain smoothed Galerkin method, 1, 2, 4 and 8 uniform sub-domains corresponding to 40, 175, 451 and 1105 nodes are used in the entire problem domain, separately. Figures 6 shows the error norms of displacement and energy with respect to the number of sub-domains. It can be seen that good convergence can be obtained in present method with condensation of degree of freedom.

6.2 Infinite plate with a hole

The problem of infinite plate with a hole subject to a unidirectional tensile load of 1.0 N/m at infinity in the x direction, as shown in Figure 7, is studied for the analysis of the dependence of computational accuracy on the number of smoothing cells. The problem has been solved for plane strain with E=1.0×10^3 N/m^2, v=0.3, a=1.0m and S=5.0m. Due to the symmetry, only the upper right quadrant of the plate is modeled, and symmetry conditions are imposed on the left and bottom edges. The analytical solution for the infinite plate is [4]

$$\begin{aligned}
\sigma_{11} &= 1-\frac{a^2}{r^2}\left(\frac{3}{2}\cos 2\theta+\cos 4\theta\right)+\frac{3a^4}{2r^4}\cos 4\theta \\
\sigma_{22} &= -\frac{a^2}{r^2}\left(\frac{1}{2}\cos 2\theta-\cos 4\theta\right)-\frac{3a^4}{2r^4}\cos 4\theta \\
\sigma_{12} &= -\frac{a^2}{r^2}\left(\frac{1}{2}\sin 2\theta+\sin 4\theta\right)+\frac{3a^4}{2r^4}\sin 4\theta
\end{aligned} \tag{37}$$

where (r,θ) are the polar coordinates and θ is measured counterclockwise from the positive x-axis. Traction boundary conditions are imposed on the edges of x=5m and y=5m based on the analytical solution of Equation (37). The displacement components corresponding to the stresses are

$$\begin{aligned}
u_1 &= \frac{a}{8\mu}\left[\frac{r}{a}(\kappa+1)\cos\theta+2\frac{a}{r}((1+\kappa)\cos\theta+\cos 3\theta)-2\frac{a^3}{r^3}\cos 3\theta\right] \\
u_2 &= \frac{a}{8\mu}\left[\frac{r}{a}(\kappa-1)\sin\theta+2\frac{a}{r}((1-\kappa)\sin\theta+\sin 3\theta)-2\frac{a^3}{r^3}\sin 3\theta\right]
\end{aligned} \tag{38}$$

where κ is defined in terms of Poisson's ratio v by $\kappa=3-4v$ for plane strain cases.

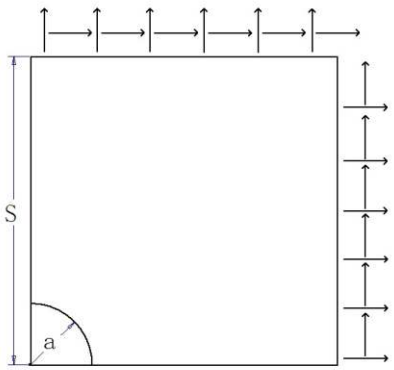

Figure 7. Infinite plate with a hole

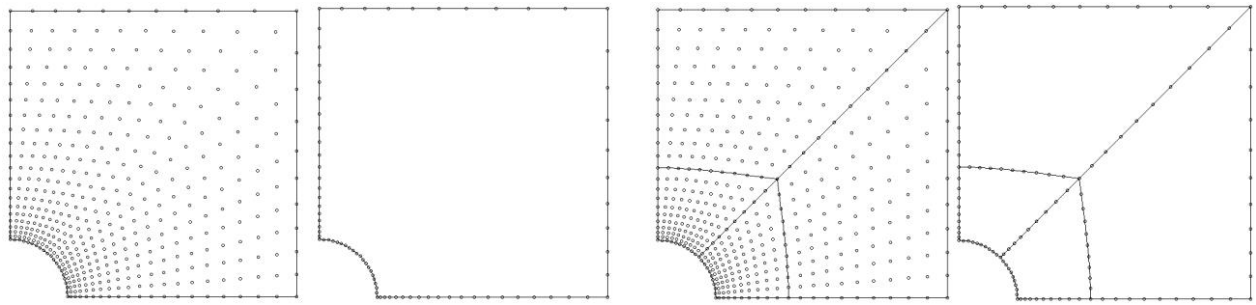

(a) 1 sub-domain (b) 4 sub-domains

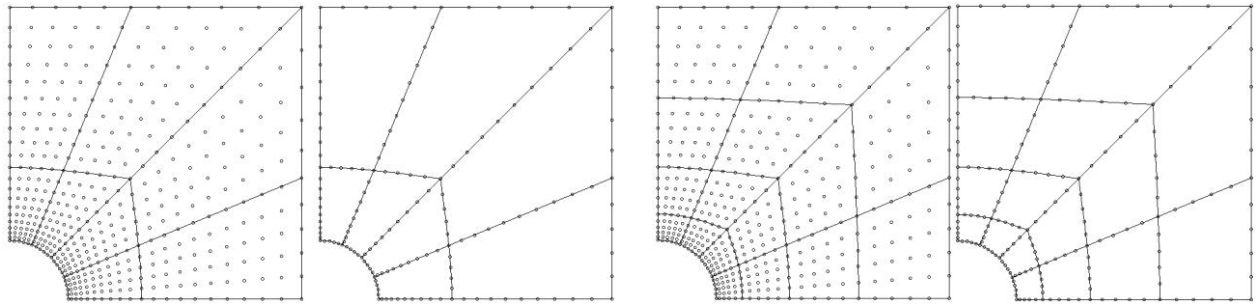

(c) 8 sub-domains (d) 16 sub-domains

Figure 8. Distributed sub-domains and nodes of infinite plate with a hole

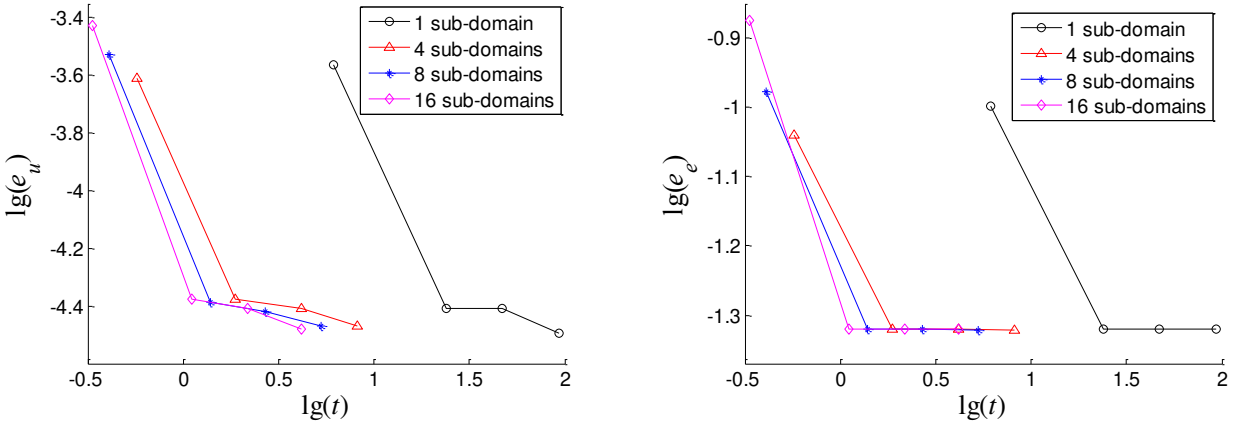

(a) Error norms of displacement (b) Error norms of energy

Figure 9. Error norms with respect to CPU time obtained by different sub-domains

In the entire problem domain, as shown in Figure 8, 441 distributed nodes are used. And 1, 4, 8, 16 sub-domains corresponding to 400, 1600, 3200 and 6400 quadrilateral smoothing cells are divided, separately. Figure 9 provides the error norms of displacement and energy with respect to the CPU time. Table 3 shows the computational costs of present method with different number of sub-domains and smoothing cells. It is observed that the more sub-domains in problems domain, the higher computational efficiency can be obtained in this case, and the present method with condensation can also improve the computational efficiency compared with those cases of without condensation. On the other hand, increasing the number of smoothing cells can improve the computational accuracy of present method, but error norms will tend to be saturated when the number of smoothing cells reaches a threshold. However, if the more number of smoothing cells for integration are used, it will consume more CPU time. Therefore, a proper number of smoothing cells is needed to balance the accuracy and efficiency of simulation. It should be further studied to understand the relationship between smoothing cells of

nodal integration and accuracy of results.

Table 3. The CPU time influenced by the number of sub-domains and smoothing cells (Unit: s)

Number of sub-domains		Number of smoothing cells			
		400	1600	3200	6400
1 sub-domain	Without condensation	6.591	24.473	48.793	96.531
	With condensation	6.132	23.901	46.889	93.803
4 sub-domains	Without condensation	0.830	2.386	4.452	8.577
	With condensation	0.571	1.882	4.168	8.134
8 sub-domains	Without condensation	0.532	1.529	2.837	5.714
	With condensation	0.410	1.380	2.706	5.274
16 sub-domains	Without condensation	0.421	1.172	2.322	4.234
	With condensation	0.334	1.105	2.179	4.160

6.3 Stress distribution in a dam

The stress analysis of a dam subjected to hydrostatic pressure on both sides of the dam, as shown in Figure 10, is studied for analysis of computational accuracy influenced by irregularly distributed sub-domains and nodes. The problems is solved for the plane strain case with E=30Gpa and v=0.15. In the dam studied, 8 irregularly distributed sub-domains with 521 distributed nodes are used for simulation, as shown in Figure 11. For nodal integration, 1120 smoothing cells are used in the entire problem domain. Numerical results of present method are compared with solutions from commercial FEM program (ANSYS), EFG method [5], RPIM method [4] and the method of reference [16]. For the purpose of comparison, the number of nodes are the same in all aforementioned methods. 1620 Gauss integration points are used for integration in EFG method, RPIM method and the method of reference [16], respectively, while 2238 midpoints (integration points) of segment of boundary Γ_L^k are used in present method. The CPU time of present method with more integration points are used to investigate the computational efficiency compared with other methods.

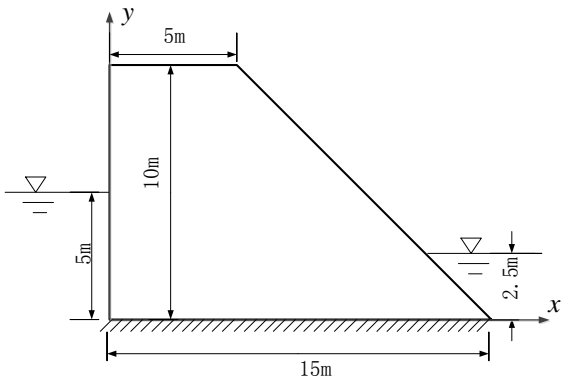

Figure 10. Water dam subjected to hydrostatic pressure

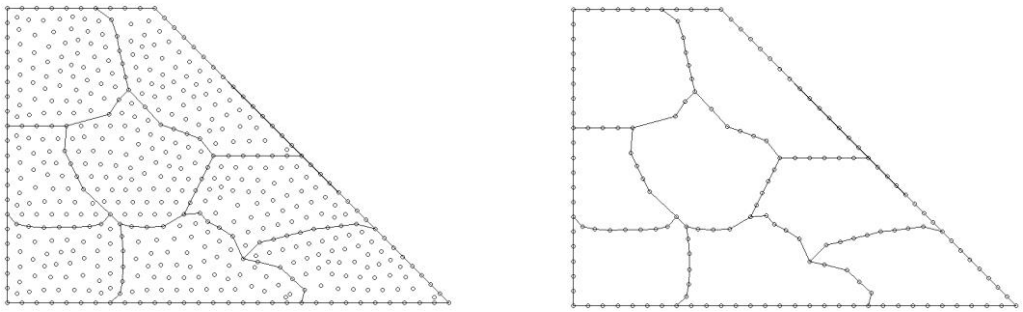

(a) Distributed nodes without condensation (b) Distributed nodes with condensation

Figure 11. Irregularly distributed sub-domains and nodes of dam

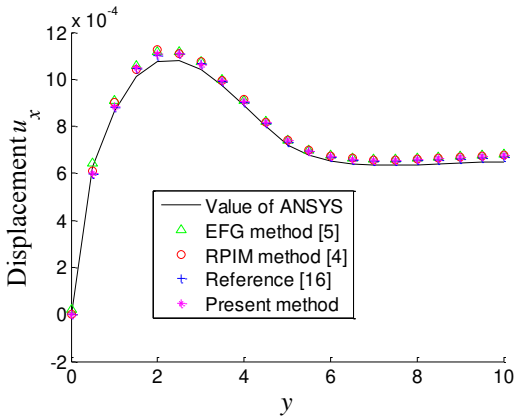

Figure 12. Displacements u_x at x=0

The displacements at x=0 are plotted in Figure 12. The results obtained by the present method with irregularly distributed sub-domains and nodes are in good agreement with those obtained by ANSYS, EFG method, RPIM method and the method of reference [16]. The distribution of stress in the dam obtained by different methods are provided in Figure 13. It can be seen that the present method with condensation of degree of freedom can also obtain good accuracy of stress distribution compare with aforementioned commonly used numerical methods. It validates that the present method works particularly well for very irregular sub-domains.

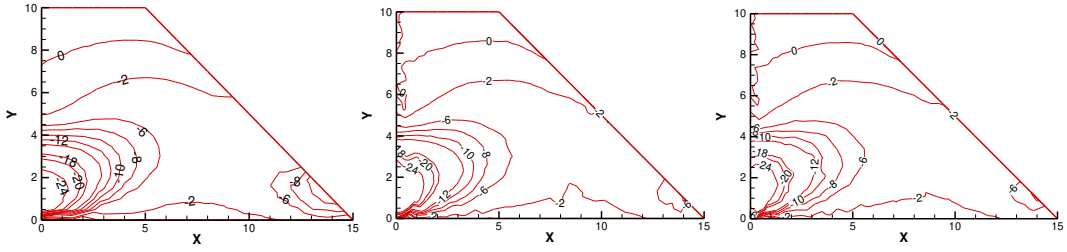

(a) ANSYS (b) EFG method [5] (c) RPIM method [4]

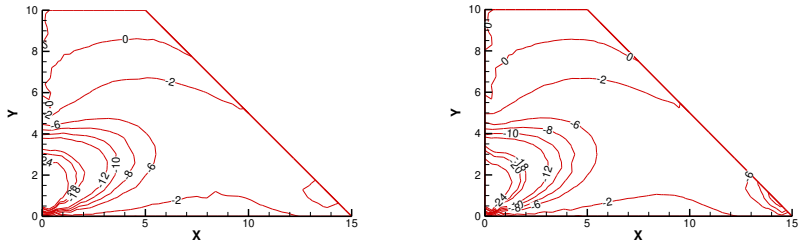

(d) Reference [16] (e) Present method with condensation

Figure 13. Distribution of stress σ_{xx} obtained by different methods (Unit: MPa)

Figure 14 shows the CPU time of EFG method, RPIM method, method of reference [16] and the present

method with condensation of degree of freedom. It can be seen that the present method with 8 sub-domains has significantly improved the computational efficiency for about 16 times compared with EFG method, even though more integration points are used in present method.

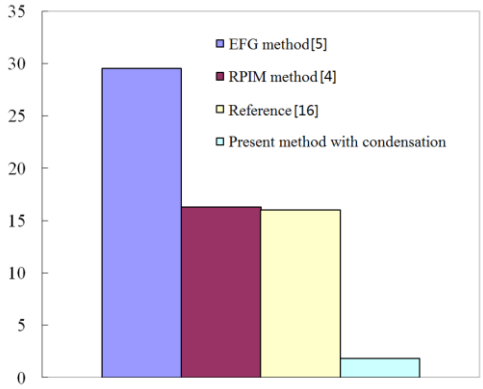

Figure 14. The CPU time of different methods (Unit: s)

7. Conclusions

In this paper, a sub-domain smoothed Galerkin method is proposed for 2D solid mechanics problems by integrating the properties of FEM and mesh-free Galerkin method, which is implemented based on the sub-domains with mesh-free nodes. The advantages of mesh-free methods are still kept in every sub-domain based on MK interpolation. Nodal integration with strain smoothing is used to simplify the calculation of sub-domains based on smoothing cells, which does not need to evaluate the mapping of integration with coordinate transformation and works particularly well for very irregular sub-domains. The local discrete equations of sub-domains are established with local search of neighbor nodes to improve the computational efficiency of MK interpolation. The global system equations are assembled with the scheme of FEM based on sub-domains.

It can be concluded from the performance of the present method in numerical examples that the sub-domain smoothed Galerkin method proposed in this paper provides an efficient and powerful tool for computational mechanics. We note without celebration that the present method is also beneficial to adaptive refinement of nodes, crack propagation problems, parallel computations of large systems, 3D solid mechanics problems and etc., which should be interesting works in the future.

Acknowledgments

Financial supports from National Natural Science Foundation of China (11272118) and ARC Future Fellowship project (FT100100172) are gratefully acknowledged. It is also partially supported by the US ARO under contract No.W911NF-12-1-0147, the NSF Grant under the award No. 1214188, and the Open Research Fund Program of the State Key Laboratory of Advanced Technology of Design and Manufacturing for Vehicle Body, Hunan University, P. R. China under the grant number 41215002.

References

[1] Liu GR, Quek SS. The Finite Element Method: A Practical Course, Butterworth-Heinemann, Oxford, 2003.

[2] Liu GR, Zeng W, Nguyen-Xuan H. Generalized stochastic cell-based smoothed finite element method (GS_CS-FEM) for solid mechanics. *Finite Elements in Analysis and Design* 2013; 63: 51-61.

[3] Belytschko T, Krongauz Y, Organ D, Fleming M, Krysl P. Meshless methods: an overview and recent developments. *Computer Methods in Applied Mechanics and Engineering* 1996; 139: 3-47.

[4] Liu GR. Meshfree methods: Moving beyond the Finite Element Method. CRC Press, Boca Raton, 2nd edition, 2009.

[5] Belytschko T, Lu TT, Gu L. Element-free Galerkin method. *International Journal for Numerical Method in Engineering* 1994; 37: 229-256.

[6] Zan Zhang, Peng Zhao, Liew KM. Improved element-free Galerkin method for two-dimensional potential problems. *Engineering Analysis with Boundary Elements* 2009; 33(4): 547-554.

[7] Louai FZ Nait-Said N, Drid S. Implementation of an efficient element-free Galerkin method for electromagnetic computation. *Engineering Analysis with Boundary Elements* 2007; 31(3): 191-199.

[8] Belinha J, Dinis LMJS. Analysis of plates and laminates using the element-free Galerkin method. *Computers & Structures* 2006; 84(22-23): 1547-1559.

[9] Wagner GJ, Liu WK. Applied of essential boundary conditions in mesh-free methods: a corrected collocation method. *International Journal for Numerical Methods in Engineering* 1999; 47:1367-1379.

[10] Kaljevic I, Saigal S. An improved element-free Galerkin formulation. *International Journal for Numerical Methods in Engineering* 1997; 40:2953-2974.

[11] Zhu T, Atluri SN. A modified collocation method and a penalty formulation for enforcing the essential boundary conditions in the element free Galerin method. *Computational Mechanics* 1998; 21: 211-222.

[12] Liu GR, Gu YT. A point interpolation method for two-dimensional solid. *International Journal for Numerical Methods in Engineering* 2001; 50 (4): 937-951.

[13] Gu YT, Liu GR. A local point interpolation method for static and dynamic analysis of thin beams. *Computer Methods in Applied Mechanics and Engineering* 2001; 190: 5515-5528.

[14] Liu GR, Gu YT. A local radial point interpolation method (LR-PIM) for free vibration analyses of 2-D solids. *Journal of Sound and Vibration* 2001; 246 (1): 29-46.

[15] Liu GR, Zhang GY, Gu YT, Wang YY. A mesh-free radial point interpolation method (RPIM) for three-dimensional solids. *Computational Mechanics* 2005; 36(6): 421-430.

[16] Lei Gu. Moving kriging interpolation and element-free Galerkin method. *International Journal for Numerical Methods in Engineering* 2003; 56: 1-11.

[17] Dai KY, Liu GR, Lim KM, Gu YT. Comparison between the radial point interpolation and the Kriging interpolation used in mesh-free method. *Computational Mechanics* 2003; 32:60-70.

[18] Lam KY, Wang QX, Li H. A novel meshless approach - Local Kriging (LoKriging) method with two-dimensional structural analysis. *Computational Mechanics* 2004; 33: 235-244.

[19] Li H, Wang QX, Lam KY. Development of a novel meshless Local Kriging (LoKriging) method for structural dynamic analysis. *Computer Methods in Applied Mechanics and Engineering* 2004; 193: 2599-2619.

[20] Bui TQ, Nguyen TN, Nguyen-Dang H. A moving Kriging interpolation-based meshless method for numerical simulation of Kirchhoff plate problems. *International Journal for Numerical Methods in Engineering* 2009; 77: 1371-1395.

[21] Bui TQ, Nguyen TN. A moving Kriging interpolation-based mesh-free method for free vibration analysis of Kirchhoff plates. *Computers & Structures* 2011; 89(3-4): 380-394.

[22] Bui TQ, Nguyen TN, Zhang CZ. A moving Kriging interpolation-based element-free Galerkin method for structural dynamic analysis. *Computer Methods in Applied Mechanics and Engineering* 2011; 200: 1354-1366.

[23] Dolbow J, Belytschko T. Numerical integration of Galerkin weak form in mesh-free methods. *Computational Mechanics* 1999; 23: 219-230.

[24] Beissel S, Belytschko T. Nodal integration of the element-free Galerkin method. *Computer Methods in Applied Mechanics and Engineering* 1996; 139: 49-74.

[25] Bonet J, Kulasegaram S. Correction and stabilization of smooth particle hydrodynamics methods with applications in metal forming simulation. *International Journal for Numerical Methods in Engineering* 1999; 47: 1189-1214.

[26] Krongauz Y, Belytschko T. Consistent pseudo-derivatives in meshless methods. *International Journal for Numerical Methods in Engineering* 1997; 146: 371-386.

[27] Chen JS, Wu CT. A stabilized conforming nodal integration for Galerkin mesh-free method. *International Journal for Numerical Methods in Engineering* 2001; 50: 435-466.

[28] Chen JS, Wu CT. Generalized nonlocal mesh-free method in strain localization. *Proceeding of International Conference on Computational Engineering Science*, Atlanta, Georgia, 6-9 October 1998.

[29] Chen JS, Wu CT, Belytschko T. Regularization of material instabilities by mesh-free approximations with intrinsic length scales. *International Journal for Numerical Methods in Engineering* 2000; 47: 1303-1322.

[30] Liu GR, Dai KY, Nguyen-Thoi T. A smoothed finite element method for mechanics problems. *Computational Mechanics* 2007; 39: 859-877.

[31] Liu GR, Nguyen TT, Dai KY, Lam KY. Theoretical aspects of the smoothed finite element method (SFEM). *International Journal for Numerical Methods in Engineering* 2007; 71: 902-930.

[32] Liu GR. A generalized gradient smoothing technique and the smoothed bilinear form for Galerkin formulation of a wide class of computational methods. *International Journal of Computational methods* 2008; 5(2): 199–236.

[33] Dai KY, Liu GR, Nguyen TT. An *n*-sided polygonal smoothed finite element method (*n*SFEM) for solid mechanics. *Finite Elements in Analysis and Design* 2007*;* 43: 847-860.

[34] Liu SJ, Wang H, Zhang H. Smoothed finite elements large deformation analysis. *International Journal of Computational Methods* 2010; 7(3): 513-524.

[35] Nguyen-Xuan H, Rabczuk T, Bordas S, Debongnie JF. A smoothed finite element method for plate analysis. *Computer Methods in Applied Mechanics and Engineering* 2008; 197: 1184-1203.

[36] Liu GR. A G space theory and a weakened weak (W2) form for a unified formulation of compatible and incompatible methods: Part I theory. *International Journal for Numerical Methods in Engineering* 2010; 81:1093-1126.

[37] Liu GR. On G space theory. *International Journal of Computational Methods*2009; 6(2): 257-289.

[38] Hu DA, Li YY, Han X, Yang G, Jiang C. A Sub-Domain RPIM with Condensation of Degree of Freedom. *Engineering Analysis with Boundary Elements* 2013; 37: 1161-1168.

[39] Hesch C, Betsch P. Isogeometric analysis and domain decomposition methods. *Computer Methods in Applied Mechanics and Engineering* 2012; 213-216: 104-112.

[40] Sengupta TK, Dipankar A, Kameswara Rao A. A new compact scheme for parallel computing using domain decomposition. *Journal of Computational Physics* 2007; 220: 654-677.

[41] Smith BF, Bjorstad P, Gropp W. Domain decomposition, parallel multilevel methods for elliptic partial differential equations. Cambridge University Press, New York, 1996.

[42] Chongmin Song. A super-element for crack analysis in the time domain. *International Journal for Numerical Methods in Engineering* 2004; 61(8): 1332-1357.

[43] Sastry CVC, Mahapatra DR, Sopalakrishnan S, Ramamurthy TS. An iterative system equivalent reduction expansion process for extraction of high frequency response from reduced order finite element model. *Computer Methods in Applied Mechanics and Engineering* 2003; 192(15): 1821-1840.

[44] Timoskenko SP, Goodier JN. Theory of elasticity. 3rd Edn, McGraw-Hill, New York, 1970.